Q. J. R. Meteorol. Soc. (2006), **132**, pp. 865–883 doi: 10.1256/qj.04.187

Observations of the depth of ice particle evaporation beneath frontal cloud to improve NWP modelling

By RICHARD M. FORBES[1]* and ROBIN J. HOGAN[2]

[1]*Met Office, Reading, UK*
[2]*University of Reading, UK*

(Received 20 December 2004; revised 21 November 2005)

SUMMARY

The evaporation (sublimation) of ice particles beneath frontal ice cloud can provide a significant source of diabatic cooling which can lead to enhanced slantwise descent below the frontal surface. The strength and vertical extent of the cooling play a role in determining the dynamic response of the atmosphere, and an adequate representation is required in numerical weather-prediction (NWP) models for accurate forecasts of frontal dynamics. In this paper, data from a vertically pointing 94 GHz radar are used to determine the characteristic depth-scale of ice particle sublimation beneath frontal ice cloud. A statistical comparison is made with equivalent data extracted from the NWP mesoscale model operational at the Met Office, defining the evaporation depth-scale as the distance for the ice water content to fall to 10% of its peak value in the cloud. The results show that the depth of the ice evaporation zone derived from observations is less than 1 km for 90% of the time. The model significantly overestimates the sublimation depth-scales by a factor of between two and three, and underestimates the local ice water content by a factor of between two and four. Consequently the results suggest the model significantly underestimates the strength of the evaporative cooling, with implications for the prediction of frontal dynamics. A number of reasons for the model discrepancy are suggested. A comparison with radiosonde relative humidity data suggests part of the overestimation in evaporation depth may be due to a high RH bias in the dry slot beneath the frontal cloud, but other possible reasons include poor vertical resolution and deficiencies in the evaporation rate or ice particle fall-speed parametrizations.

KEYWORDS: Midlatitude fronts Numerical weather prediction Snow sublimation

1. INTRODUCTION

Observational and modelling studies of cooling due to the evaporation of hydrometeors in the atmosphere have highlighted the importance for the dynamics of cloud systems, from small-scale microbursts and squall-line downdraughts (e.g. Thorpe *et al.* 1982; Srivastava 1985; Johnson *et al.* 1993), to large-scale midlatitude fronts (Thorpe and Clough 1991; Clough and Franks 1991; Parker and Thorpe 1995; Clough *et al.* 2000; Forbes and Clark 2003). For operational mesoscale numerical weather-prediction (NWP) models, the forecasting of wind and precipitation associated with fronts is of key importance in midlatitudes and so a relevant question is whether the models can appropriately represent the dynamical impact of the hydrometeor evaporation beneath stratiform ice cloud. Although both rain and snow evaporation can occur in a frontal region, Clough and Franks (1991) suggested that evaporative cooling from falling ice particles can have a more significant dynamical impact than rain due to the relatively rapid evaporation of snow in a shallow layer. The relative efficiency of evaporation of ice particles is due to their lower bulk density and lower terminal fall velocity. Modelling studies of the evaporation zone by Heymsfield and Donner (1990) and Clough and Franks (1991) both show that evaporation depths for snow can be significantly less than those for rain in typical frontal regions.

The evaporative cooling confined to a shallow layer directly beneath the ascending frontal flow modifies the static stability, intensifying the potential vorticity dipole across the front, which enhances the transverse slantwise frontal circulation due to

* Corresponding author: Met Office, Joint Centre for Mesoscale Meteorology, University of Reading, Earley Gate, PO Box 243, Reading, Berkshire RG6 6BB, UK. e-mail: richard.forbes@metoffice.gov.uk

increased frontogenetic forcing and possibly moist symmetric instability (Clough *et al.* 2000; Forbes and Clark 2003). Parker and Thorpe (1995) used a two-dimensional (2D) semi-geostrophic model with a simple parametrization of ice evaporative cooling in a prescribed region beneath the frontal updraught and showed that evaporation of ice led to a stronger frontal downdraught. The importance of these downdraughts was highlighted in a study by Browning (2004) of the 1987 cyclone that caused great damage to the southern UK. Browning suggested that evaporative cooling in the dry slot beneath stratiform ice cloud near the tip of the cloud head may play a role in enhancing the strong winds at the surface. The reduction in low-level static stability could lead to strong turbulence in a region of low Richardson number, mixing high winds down to the surface, or even trigger upright convection bringing high-momentum air closer to the ground.

The evidence suggests that the thermodynamic aspects of the frontal evaporation zone need to be represented appropriately in NWP models in order to predict the dynamics of fronts in midlatitude cyclones, but there has been little validation of the microphysics in frontal evaporation zones in operational NWP models. For a reliable evaluation, a comparison of the model with observations for a large number of forecasts is required, but the number of *in situ* observations from aircraft and sondes is relatively limited. Cloud radars, on the other hand, can provide long time series of reflectivity data with information on the hydrometeors present in the atmosphere. This paper describes a technique to use data from a vertically pointing cloud radar to assess the representation of the evaporation zone beneath stratiform ice cloud in an NWP model.

The primary quantities that determine the local cooling rate and depth of the evaporation zone are the flux of ice into the subsaturated layer and the rate of evaporation. The latter depends on the magnitude of the subsaturation as well as other factors such as the degree of particle ventilation. The two quantities that can be inferred from vertical profiles of radar reflectivity are the ice water content (IWC) and depth-scale of evaporation, which can then be used to assess the representation of the evaporation zone in the NWP model. The radar data used in this study is a year-long time series of data from a vertically pointing 94 GHz radar based at Chilbolton in the south of the UK—appropriate for observing ice particles in the atmosphere. The model used in this study is the mesoscale version of the Met Office Unified Model operational at the time. Statistics of the evaporative depth-scale, estimated IWC, and other characteristics of the frontal evaporation zone are extracted from the data and compared with equivalent statistics from a time series of forecasts from the operational Unified Model for the same time period.

Section 2 describes the characteristics of the radar data and the NWP model. Section 3 describes the method used to extract regions of ice evaporation, the assumptions that are made and calculation of ice evaporation depth-scales. Section 4 presents results from the statistical analysis of evaporating profiles from the radar and model data, and assesses whether part of the difference in the results can be attributed to a relative humidity (RH) bias in the model. Section 5 provides a discussion and a summary of the results follows in section 6.

2. Radar and NWP model data

(*a*) *94 GHz radar*

The observational dataset is a time series of radar reflectivity profiles from the 94 GHz (3.2 mm wavelength) 'Galileo' vertically pointing cloud radar based at the Chilbolton Radar Facility in Hampshire, UK (51.14°N, 1.44°W). The radar reflectivity

observations used in this study are 30-second averages (which, for a wind speed of 20 m s^{-1}, corresponds to a resolution of 600 m in the horizontal). The vertical resolution of the data is 60 m. A description of the estimation of IWC and determination of the minimum detectable IWC follows.

(i) *Estimation of ice water content from reflectivity.* A variety of relationships between IWC and reflectivity (Z) have been proposed based on ice size spectra data from aircraft (Sassen 1987; Atlas *et al.* 1995; Brown *et al.* 1995). Such relationships take the form $\mathrm{IWC} = a' Z^{b'}$, where the IWC is in g m^{-3} and the reflectivity factor is in $mm^6 m^{-3}$, or equivalently $\log_{10}(\mathrm{IWC}) = a'' Z + b''$ where IWC is in g m^{-3} and Z is in dBZ. The constants a', b', a'' and b'' are determined by a least-squares fit to the IWC and Z data calculated from the observed ice spectra, and a wide range of values have been reported. Liu and Illingworth (2000, subsequently referred to as LI2000) showed that IWC–Z relations derived from different datasets by different authors did show a degree of consistency if the same assumptions of particle density and radar frequency were used. However, the uncertainty in the value of IWC derived from an individual Z measurement is about a factor of 2 (i.e. +100% and −50%). Brown *et al.* (1995) suggested that an independent measure of mean ice particle size, for example from coincident lidar observations (Intrieri *et al.* 1993) or dual-frequency radars (Hogan *et al.* 2000), could reduce the error in IWC to a factor of +50% and −30%. LI2000 showed that a similar reduction in the error can be achieved if temperature, rather than mean particle size, is used in addition to the reflectivity. Temperature has the advantage that it is obtainable from a forecast model to within the required accuracy of 6 K. The correlation between temperature and mean diameter is based on the evidence that ice crystal size spectra observed at higher temperatures tend to contain an increasing fraction of large particles leading to higher values of the mean particle diameter (Heymsfield and Platt 1984). A simple explanation is that the aggregation process shifts the size spectrum towards larger particles at greater distances from cloud top and higher temperatures.

LI2000 calculated IWC–Z relationships for different temperature ranges from Met Office C-130 aircraft data during flights of the European Cirrus and Radiation Experiment (EUCREX) for a radar frequency of 94 GHz. The EUCREX dataset comprises a total of 7000 5-second-averaged size spectra from airborne PMS 2D-C and 2D-P particle probes along approximately 5100 km of flight through frontal ice cloud around the UK between temperatures of 0 °C and −55 °C (Brown *et al.* 1995). Reflectivity values calculated from the observed ice spectra range from −50 dBZ to 10 dBZ and so any derived IWC–Z relationship is valid for reflectivities within this range. LI2000 assumed an ice particle density, ρ, was dependent on diameter, D, as used by Brown and Francis (1995) and Atlas *et al.* (1995), i.e.

$$\rho = 0.07 D^{-1.1}, \tag{1}$$

where ρ is in g cm^3, D is in cm, or equivalently,

$$m = 0.0185 D^{1.9}, \tag{2}$$

where m is the mass of a particle of size D. Separate IWC–Z equations were then calculated for 6 K temperature bins. One problem with incorporating the temperature dependence in this way is that retrieved IWC fields tend to have discontinuities at the 6 K boundaries.

To overcome this problem, the EUCREX data have been re-analysed in a similar way to LI2000 but fitted with a smooth function for IWC based on both Z and the

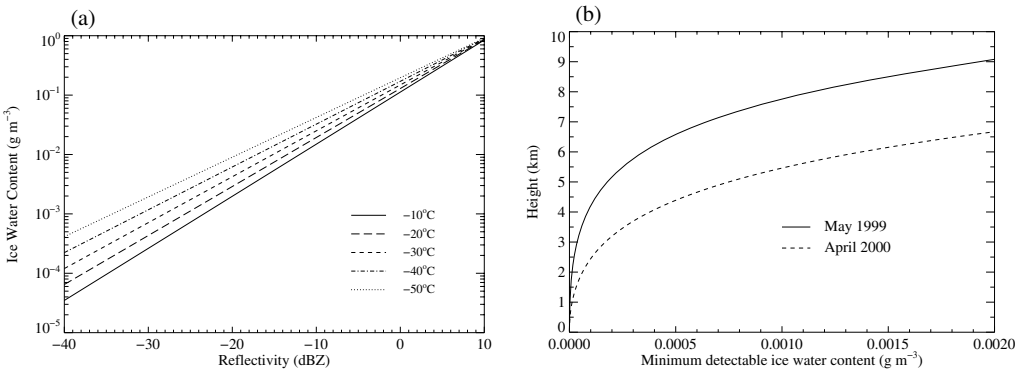

Figure 1. (a) The dependence of ice water content (g m^{-3}) on radar reflectivity factor (dBZ) for a range of temperatures using Eq. (3) derived by Hogan *et al.* (2006) from aircraft data (Liu and Illingworth 2000). (b) Variation with range (height) of the estimated minimum detectable ice water content (g m^{-3}) for the Chilbolton 94 GHz cloud radar during the months of May 1999 and April 2000 (the start and end of the observation period) due to the inverse square law and gaseous attenuation (using the year-average model temperature and humidity profiles).

temperature, T. The analysis relies on the accuracy of the particle size spectra from the aircraft probes, particularly for the larger particles, in order to calculate a reliable value of radar reflectivity. To test the validity of the calculation of reflectivity from the observed spectra, estimates of radar reflectivity from the aircraft particle size spectra were compared with coincident reflectivity data from a 3 GHz radar for five Met Office C-130 flights. The comparison is described in Hogan *et al.* (2006, hereafter referred to as H2006) and the results suggest that there is no significant undersampling of large particles and that radar reflectivity may be reliably calculated from size spectra from the aircraft in midlatitude stratiform clouds.

For a 3 GHz radar, Rayleigh theory can be used for the calculation of radar reflectivity, but at 94 GHz the diameter of the larger particles may be an appreciable fraction of the radar wavelength, resulting in a decrease in the backscatter compared to that predicted by the Rayleigh approximation. A correction based on Mie theory is used in the calculation of the radar reflectivity for the analysis in this paper. H2006 describe the derivation of the IWC(Z,T) relationship in detail. Essentially, once the IWC and Z values have been calculated for the whole dataset of observed ice particle spectra, the mean IWC in logarithmic space is calculated for each 5 dB range of Z and each 5 K temperature bin, followed by calculation of the least-squares fit in logarithmic space. The reader is referred to H2006 for more detailed information.

The function for IWC resulting from the above analysis, and used in this paper, is

$$\log_{10}(\mathrm{IWC}) = 0.00052ZT + 0.0929Z - 0.00605T - 1.01, \qquad (3)$$

where IWC is in g m^{-3}, Z is in dBZ, and T is in °C. This provides a smoothly varying function that represents the variation of the IWC–Z relationship with temperature found by LI2000 and it is this equation that is used here with temperature data taken from the Met Office operational NWP model. Figure 1(a) illustrates the dependence of IWC on Z in Eq. (3) for a range of temperatures. Note that the equivalent relationship derived in H2006 is from a later version of the data analysis which performs the initial fit of IWC for each reflectivity bin in linear rather than logarithmic space, giving 20% higher IWC for a given value of Z.

Another important aspect of the above analysis relevant to this paper is the applicability of Eq. (3) to evaporating ice particles in subsaturated air, when the measurements were obtained from a variety of ice clouds which were more than likely in ambient conditions of ice saturation or above. Observations in the laboratory (Nelson 1998) and from aircraft replicator data (Heymsfield and Miloshevich 2003) show that ice crystals become rounded structures when evaporating, resulting in particles with a higher bulk density. Higher values of both a and b in the mass–dimension relationship ($m = aD^b$; Eq. (2)) are therefore likely. Also the small particles evaporate quickly, leaving fewer small particles relative to the number of larger particles. The effects of these uncertainties on the IWC–Z relationship are discussed in H2006 (Eq. (13) in section 4 and Eq. (17) in the appendix). A higher value of b and a lower number concentration intercept, N_0, for the particle size distribution that might occur in a sublimation zone both act to reduce the IWC for a given Z. Taking the extreme of solid spherical ice particles ($b = 3$), the IWC for a given Z could be a factor of two less, but the discrepancy is likely to be much less than this. The potential impact of uncertainties in the IWC(Z,T) relationship on the evaporative depth-scale results are discussed in section 3(f).

(ii) *Minimum detectable reflectivity/ice water content.* In an evaporation zone, the reflectivity decreases with decreasing height, and knowledge of the minimum reflectivity detectable by the radar at a particular height is required in order to define and determine an evaporative depth-scale. The minimum detectable reflectivity at a range R (in km) for the radar can be calculated using

$$Z_{\min}(\mathrm{dBZ}) = 20\log_{10}(R) - k + A(R). \tag{4}$$

The first term on the right-hand side represents the decrease in returned power with range due to the inverse-square law. k is a calibration constant for the 94z GHz radar at Chilbolton which increases with time from 2 to 14 dB ($\pm$1.5 dB) due to degradation of the radar transmitter power during 1999 and 2000 (Hogan *et al.* 2003). A is the two-way attenuation due to gaseous (water vapour, oxygen) and liquid absorption to range R. Large liquid water drops (i.e. rain) cause the most significant attenuation of the radar signal and the most uncertainty, so any profiles that are considered to contain liquid water cloud or rain are not used in the analysis. In the absence of liquid water, the attenuation is dominated by water vapour. Generally the amount of water vapour in the atmosphere decreases with height, so the vertically integrated effect on Z due to gaseous attenuation increases rapidly with height in the lower troposphere and levels off to a maximum of between 1 and 4 dB (depending on season) in the upper troposphere. The gaseous attenuation was estimated with the model of Liebe (1985) using temperature, pressure and water vapour profiles over the Chilbolton site from the operational mesoscale model (see the following subsection for the model details). Ice cloud attenuation can be neglected over the distance of the evaporation depth. The variation of the minimum detectable IWC from the 94 GHz radar with time and height is calculated from Eqs. (3) and (4) and is illustrated in Fig. 1(b).

(*b*) *NWP model*

The quasi-hydrostatic version of the Unified Model (Cullen 1993) operational at the Met Office in 1999 and 2000 is used in this study. The mesoscale NWP model covering the UK has a horizontal grid resolution of 0.11° on a rotated grid (which corresponds to an approximate horizontal grid length of 12 km) and 38 hybrid pressure levels in the vertical with mid-tropospheric layer depths varying from 500 to 750 m. In common with many other operational NWP systems, the model uses a bulk microphysics scheme

with a limited set of prognostic water variables, namely vapour, cloud liquid water and cloud ice. The microphysics parametrization is described in Wilson and Ballard (1999) and represents a range of microphysical warm rain and ice phase transfer processes described by physically based equations. The aspects of the parametrization with most relevance for this study are described below. The reader is referred to Wilson and Ballard (1999) for a more complete description of the scheme.

(i) *Ice water content as a prognostic variable.* In common with many other atmospheric models, the Unified Model has a single-moment representation of ice in a grid box and the prognostic variable is grid-box mean ice specific humidity, q_i (kg kg^{-1}), which sediments and is advected by the 3D wind field. q_i can be defined by the integral of particle mass over the particle size spectrum, where the mass–diameter relationship is $m(D) = aD^b$ and the number concentration is parametrized as an exponential function, $N(D) = N_0 f(T)\exp(-\Lambda D)$. The constants in the mass–diameter relationship are $a = 0.069$ and $b = 2.0$, N is the number concentration of ice particles with diameters between D and $D + \mathrm{d}D$, N_0 is fixed at 2.0×10^6, $f(T)$ is a function of temperature T, and Λ is the slope of the exponential distribution calculated from the total mass of ice in the grid box.

(ii) *Ice terminal fall-speed parametrization.* The terminal fall speed of an ice particle is specified as $v_\mathrm{t}(D) = cD^d$ with constants $c = 25.2$ and $d = 0.527$. For each model grid box at each time step, the ice particle size distribution is calculated from the mass of ice in the grid box, and the fall-speed equation is integrated over the mass spectrum to give the bulk (mass-weighted) fall speed. This is then used to calculate the amount of mass sedimenting to the grid boxes below.

(iii) *Ice evaporation rate parametrization.* The rate of change of mass of a single ice particle due to evaporation (or vapour deposition) can be written as

$$\frac{\partial m}{\partial t} = 4\pi C G s_\mathrm{i} F, \tag{5}$$

where C is the particle shape factor, G is a term that depends upon temperature and pressure, s_i is the supersaturation with respect to ice, and F is the ventilation coefficient. For each model grid box at each time step, the rate equation is integrated over the ice particle size spectrum to give the total deposition/evaporation rate for the model, transferring mass between the solid and vapour phases.

(iv) *Extraction of model data.* For this study, instantaneous vertical profiles are extracted from the model at the location of the Chilbolton radar every hour from a series of 6-hour forecasts to form a continuous hourly dataset equivalent to the time series of IWC from the radar, from May 1999 to April 2000. There are only 24 vertical profiles per day from the model, considerably less than are available from the observations. However, the model fields are much smoother in time than the observations and the lower sample size from the model is considered to be as representative as a larger sample from the observations. The next section describes further processing of the data to extract information on the evaporation zone.

3. Method for calculating ice evaporation depth-scales

(*a*) *Definition of an evaporative depth-scale*

The aim is to extract profiles from regions of frontal cloud with ice particles falling and evaporating into drier air beneath. Radar-derived IWC is the only relevant observed

variable available during the time period and an evaporating zone can therefore only be defined in terms of the profile of IWC. Although intermittent RH profiles are available from radiosondes 25 km away from the radar, the data are too sparse in time to be of direct use in the extraction method.

Each profile is analysed in turn and an evaporation zone is defined as any region in which there is a decrease in IWC with decreasing altitude. There are two main assumptions for this to be valid. Firstly, the evaporation zone in the profile must be in a region that is horizontally spatially homogeneous to avoid spurious results from intersecting individual parabolic fall streaks. This is addressed by averaging the data in time and using data only from regions that are spatially coherent, as discussed in more detail in subsections 3(b) and 3(e) below. Secondly, the profile is assumed to be in a steady state, i.e. the time-scale for individual particles to evaporate is less than the time for other characteristics of the profile to change, such as changes in the RH regime and cloud-base lowering. If we assume an evaporation depth of 500 m, and an average ice particle fall speed of 0.5 m s^{-1}, then the time-scale for the ice particle to pass through the layer (and evaporate) is 1000 s. The time-scale for the cloud to lower by 500 m is related to the moistening rate which is likely to be much slower (i.e. a few hours). Harris (1977) performed 1D numerical experiments with a model of the ice evaporation zone for a range of different humidities and snowfall rates, and showed that the cloud-base lowering rate was between 60 m and 180 m per hour. Hence the time-scale for individual particles to fall and evaporate in the profile is substantially less than the time-scale for the profile to change significantly, which supports the validity of the steady-state assumption.

The depth-scale of the evaporation zone is defined as the difference between the height of the maximum IWC and the height at which the IWC falls to a specified fraction of the maximum value. This definition, formulated in relative terms, is much less susceptible to IWC errors than an absolute definition, but still provides useful information on the depth of evaporation zone. In this study, the relative fraction is set to 10%, i.e. 90% of the mass of ice evaporates within the depth-scale of the evaporation zone. For the purpose of comparison between the radar observations and the model, the choice of definition is not crucial as long as the same definition is used for both.

(*b*) *Horizontal averaging (radar data only)*

The vertical profiles from the radar are 30-second averages. After conversion from reflectivity to IWC, further time averaging of the profiles is performed to reduce the impact of small-scale variability and slantwise fall paths due to vertical wind shear, and to enable a fairer comparison between the observations and the model (which has a grid spacing of 12 km). Horizontal wind speed data from the model at the observation times are used to average the 30-second radar IWC profile time series linearly in time to regular horizontal distance intervals. Ideally the horizontal wind speed in the evaporating zone should be used for the averaging, but this is available only for a small proportion of the dataset and, for simplicity, vertical averages of the horizontal wind over the depth of the troposphere are used. Tests show that the precise choice of wind field used in the horizontal averaging does not affect the main results in this paper.

Figure 2 shows the effect of horizontal averaging on the radar data for a particular day in 1999 in which a front with significant evaporating ice cloud passed over Chilbolton. The fall streaks from individual generating cells in the upper region of the frontal cloud are apparent in the 1 km resolution data, although the cloud base is often considerably more uniform (Fig. 2(a)). However, the evaporative depth-scale calculation

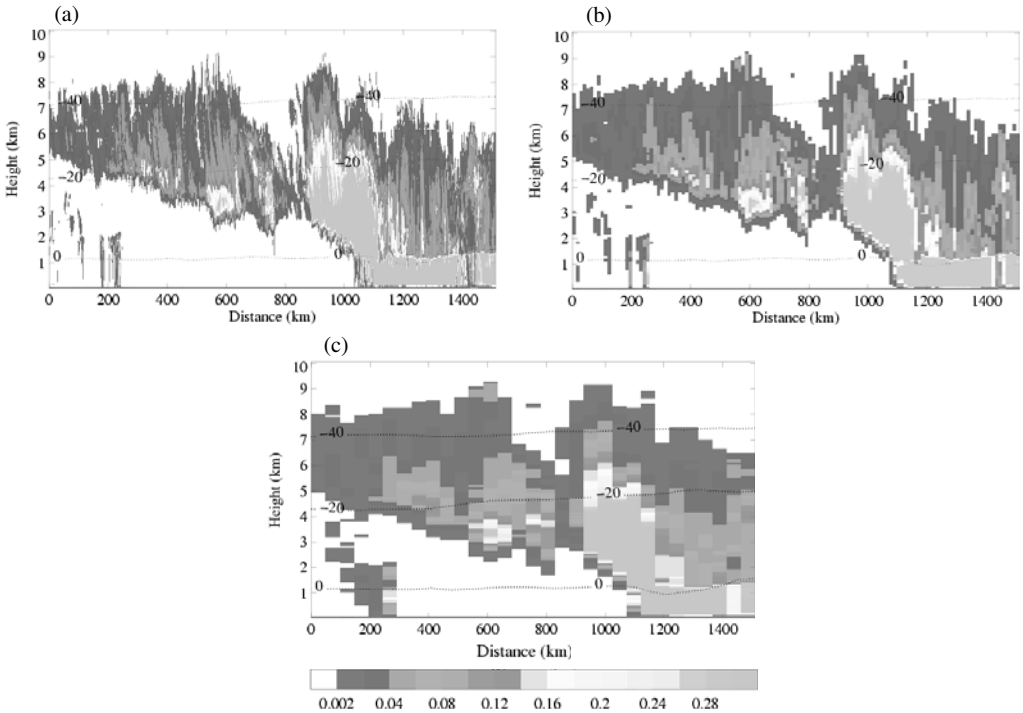

Figure 2. Ice water content (shading, g m^{-3}) vertical profile time series for 2 April 2000 (converted to a distance coordinate) for 94 GHz radar data horizontally averaged to (a) 1 km, (b) 12 km, and (c) 48 km. Temperature contours (°C) from the model are overlaid (dotted lines). Ice water content values are valid only for temperatures below 0 °C. Values at temperatures above freezing are included only to indicate the area of rain.

assumes that the ice remains in a model grid box as it falls and so further averaging is advantageous. For a wind shear of 10 m $s^{-1}km^{-1}$ in the vertical, the horizontal wind drift of ice particles falling at 1 m s^{-1} over a 1 km depth will be 10 km, so horizontal averaging of at least this scale is desirable. On the other hand, averaging over too great a distance will introduce errors in the depth-scale due to the sloping characteristics of frontal cloud (Fig. 2(c)). For a frontal ice cloud slope of 1 in 100, the overestimation of evaporation depth for the 10 km averaged data is 100 m, and this increases linearly with increasing horizontal averaging and increasing slope of the frontal surface. An averaging distance of 12 km is chosen to be consistent with the grid resolution of the model data (Fig. 2(b)).

(*c*) *Removing liquid water attenuated profiles (radar data only)*

The radar signal is corrected for attenuation by water vapour (estimated from the model), but a correction for attenuation by liquid water is much more difficult due to uncertainty in the location and amount of liquid water in the atmosphere. Fortunately, for the majority of cases there is little cloud beneath the evaporating upper-level cloud. However, to remove uncertainty due to liquid water attenuation, all profiles in which there is rain (identified by high reflectivity below the freezing level), or low-level cloud (warmer than −10 °C) beneath an evaporating zone, are excluded. Fox and Illingworth (1997) showed that stratocumulus cloud more than about 200 m thick produce drizzle which would be detectable by the 94 GHz radar and

O'Connor (personal communication) has shown that the radar can detect stratocumulus liquid water paths down to 150 g m^{-2}. The attenuation at 94 GHz due to absorption in the Rayleigh regime is approximately 4 dB km^{-1} (g $m^3)^{-1}$ (Liebe *et al.* 1989). This suggests that the maximum attenuation due to liquid water clouds that are not detected by the radar will be around 1 dBZ. A reflectivity error of this magnitude may decrease the observed IWC by up to 20% but the whole IWC profile in the evaporation zone is affected and the evaporative depth-scale defined in relative terms does not change significantly. (See section 3(f) for a discussion of the impact of reflectivity errors on the evaporative depth-scale.)

(*d*) *Minimum ice water content*

To be able to calculate the evaporation depth-scale as defined earlier, the whole evaporating profile—from the top of the evaporation zone to the point at which there is only 10% of the ice remaining—must be present in the data. As discussed in section 2(a), the radar has a minimum detectable reflectivity defined by Eq. (4) which, using Eq. (3), converts to a minimum detectable IWC dependent both on height and time (Fig. 1(b)). At the end of the data period (April 2000), the estimated minimum detectable IWC is at its highest, and below a height of 7 km is 0.002 g m^{-3} (equivalent to $Z = -26$ dBZ at $-40\,^{\circ}$C). Following the definition of the evaporation depth-scale, in order to observe the whole profile the IWC at the top of the evaporating profile must be greater than 0.02 g m^{-3} and all profiles should therefore be observable with this criterion. The same minimum IWC rule is applied to both the radar and the model data.

(*e*) *Defining a region of ice cloud evaporation*

As discussed earlier, the IWC must decrease with decreasing height from the maximum to 10% of the maximum at an altitude higher than the 0 °C level, i.e. the whole profile must be below freezing. If the IWC increases with decreasing height at any point then the profile is discarded. In the radar data, any isolated profiles are discarded if they are more than 24 km away from the next profile or if the height of the top of the evaporation zone is more than 1 km different from profiles either side.

There is a further condition that the IWC maximum (calculated from the reflectivity) must be at an altitude higher than 500 m above the 0 °C isotherm (obtained from the model). The model height of the 0 °C isotherm has been shown to have an r.m.s. error of 150m and an overall bias of less than 20 m (Mittermaier and Illingworth 2003).

Figure 3 shows an example of frontal cloud from the 12 km averaged radar data. The vertical bars mark the extent of the evaporation zone for profiles that have been extracted using the above method.

(*f*) *Impact of reflectivity and IWC–Z relationship errors*

Equation (3) is primarily a function of reflectivity and only a weak function of temperature, so the dominant impact of data errors is from the reflectivity observations. A bias of +2 dBZ in the reflectivity gives a bias in the IWC close to a factor of 1.5 at a temperature of $-20\,^{\circ}$C. This increases to a factor of 2.1 for a reflectivity bias of +4 dBZ. Despite a significant impact on the IWC, a constant bias in Z does not change the evaporative depth-scale defined in relative terms because all ice water contents are multiplied by the same factor. There is, however, a small impact on the evaporative depth-scale if there is a Z-dependent bias which could be due to an incorrect IWC–Z relation. As an example, an IWC–Z relationship from Sassen (1987), who analysed data from various sources, is compared with Eq. (3) for a temperature of $-20\,^{\circ}$C.

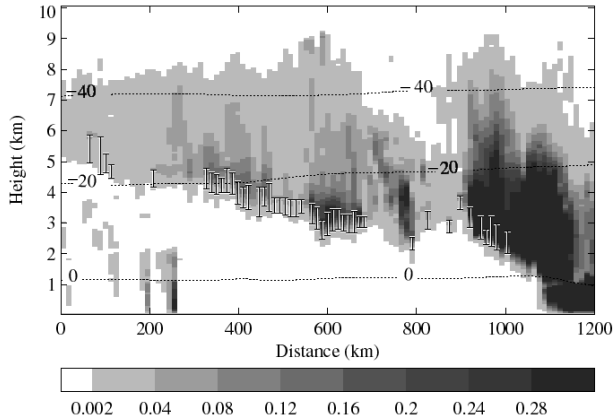

Figure 3. Ice water content (shading, g m^{-3}) calculated from the 94 GHz radar averaged to 12 km, for a frontal cloud event on 2 April 2000. The profiles that contain a region of evaporating ice are shown with a vertical bar, the vertical extent of which defines the evaporation depth. Temperature contours (°C) from the model are overlaid.

The relationships are

$$\text{IWC} = 0.129Z^{0.825} \quad \text{from Eq. (3) for } T = -20\,^{\circ}\text{C}$$
$$\text{IWC} = 0.037Z^{0.7} \quad \text{from Sassen (1987).}$$

The IWC–Z relationship in Sassen (1987) is based on Rayleigh theory and thus overestimates the reflectivity for a given IWC when applied in the Mie regime for a 94 GHz radar (particularly at higher temperatures where larger particles may be present). Thus, for a given Z, the IWC is underestimated by the Sassen relationship compared to Eq. (3), but is used here as an example to highlight the impact of a possible Z-dependent bias on the derived evaporative depth-scales.

For a reflectivity profile that decreases linearly with height from 0 dBZ at the top of the evaporative zone, the difference between the evaporative depth-scale from the above relationships is only 20%, even for this example comparison in which the IWC at 0 dBZ differs by a factor of three. This suggests the evaporative depth-scales derived from the radar will have an error of less than 20%, even if the IWC is in error by a factor of two due to incorrect assumptions about the ice particle density in the evaporation zone, as discussed in section 2(a).

4. Results

(*a*) *Comparison between the model and radar evaporation depth-scales*

The method to extract evaporating ice profiles is applied to one year (May 1999–April 2000) of radar and model data at 12 km resolution. The radar dataset contains approximately 40 000 12 km averaged vertical profiles, of which just under 2000 (∼5%) are extracted as profiles with ice evaporation. The model dataset contains 7000 profiles of which 315 (∼5%) include regions of evaporation. The number of different events in the dataset (i.e. fronts passing over the radar) is estimated to be around 70, although the exact number depends on the precise definition of an ‘event’.

Figures 4(a) and (b) show the probability density of different evaporative depth-scales from the 12 km averaged radar data binned into 120 m depth ranges (half the vertical resolution of the data) and 500 m depth ranges (for comparison with the model).

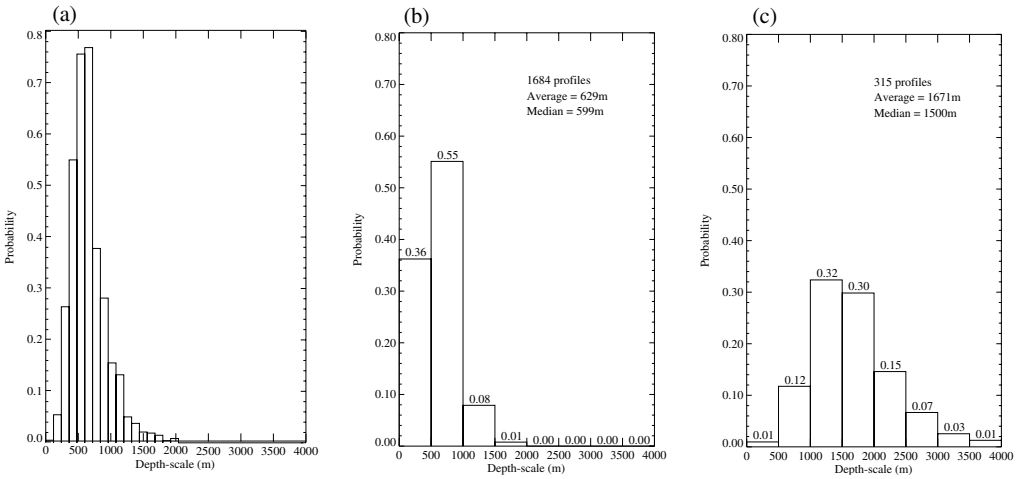

Figure 4. Probability distribution (i.e. frequency of occurrence) of ice evaporative depth-scale for May 1999 to April 2000 over Chilbolton from (a) radar observations averaged to 12 km binned into 120 m depth intervals, (b) the same radar observations binned into 500 m depth intervals, and (c) the 12 km mesoscale model results binned into 500 m depth intervals.

The average evaporative depth-scale is approximately 630 m. Over 90% of the profiles have an ice evaporative depth-scale of less than 1 km and there are no profiles with a depth-scale over 2 km. The effect on the depth-scale of averaging the data to 48 km, rather than 12 km, is small; the average increases by only 10% to 700 m.

A comparison between the observations and the model results (Figs. 4(b) and (c)) shows the model probability distribution shifted towards significantly higher evaporation depth-scales. The average evaporation depth for the model is approximately 1670 m, overestimating the radar average depth-scale by a factor of more than 2.5. Although there is some variation from day to day, the distributions of evaporative depth-scale and the difference between the model and the radar data are reasonably robust for individual fronts. The daily average evaporative depth-scales from an analysis of radar and model data for days with evaporating frontal cloud in October, November and December 1999 are shown in Fig. 5.

Figure 6(a) shows the distributions of ice water content at the top of the evaporation layer for both the radar observations and the model. The average IWC for the observations is 0.150 g m^{-3}, with a possible error of up to a factor of two, but the average IWC for the model is only 0.044 g m^{-3}. Even taking into account an overestimate in the observation-derived IWC, the comparison highlights the significant underestimate of ice from the model in the evaporating region of fronts. The IWC bias is of interest in itself for model evaluation, but the difference also has an implication for the evaporative depth-scale comparison. For an evaporating profile to be included in the extracted dataset, the minimum IWC at the top of the evaporating zone had to be greater than 0.02 g m^{-3} (see section 2(a)). However, if the model has significantly less ice than that derived from the radar, then a bias may be introduced into the evaporative depth-scales, although the error analysis in the previous section suggests any effect is likely to be small. To estimate the impact of a difference in IWC, the same analysis was performed on the 1-year time series of data from the model with an IWC cut off four times lower, i.e. 0.005 g m^{-3}. The number of extracted profiles increased to 900, but the average evaporative depth-scale decreased by only 6% to 1560 m.

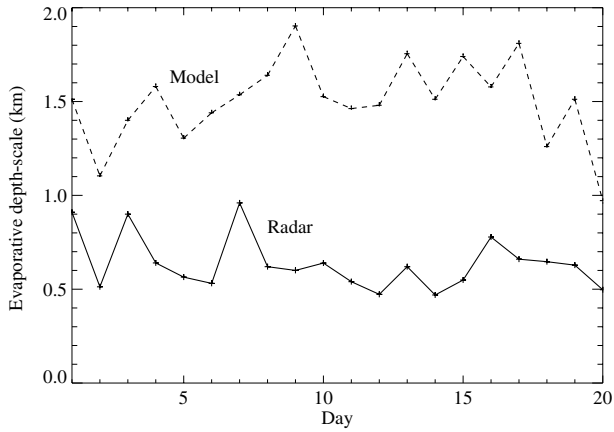

Figure 5. Model- and radar-derived daily averaged evaporative depth-scales for 20 separate days during October, November and December 1999 in which frontal ice cloud evaporation was present.

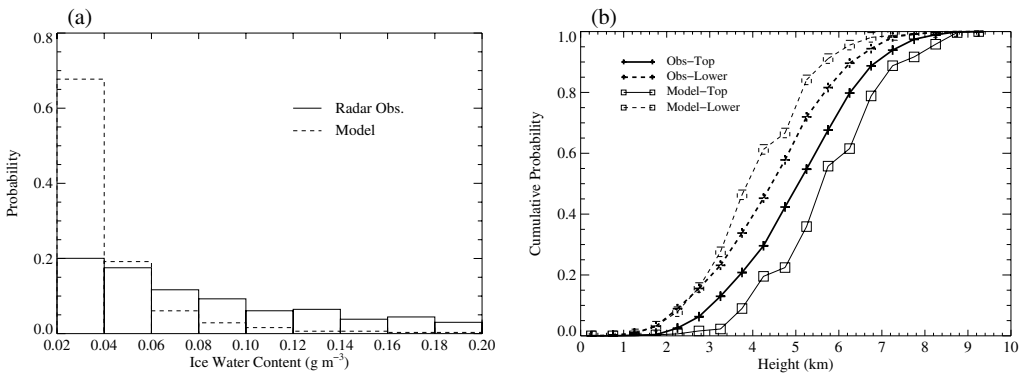

Figure 6. Probability distributions for one year of ice evaporation profile data for both the 12 km averaged radar observations and the model: (a) probability distribution of ice water content (g m^{-3}) at the top of the evaporation layer, and (b) the cumulative probability distribution of altitude for the upper and lower bounds of the evaporation layer.

The above results are based on data from the first six hours of the model forecasts and it is possible that the model takes a certain amount of time to adjust from the initial state (i.e. spin-up). To test the impact of any spin-up problems on the results, the statistics were recalculated using model data from 6 to 12 hours into the forecast. The year-average evaporative depth-scale decreased by only 4% to 1607 m and the average ice water content at the top of the evaporation layer increased by 11% to 0.049 g m^{-3}. The changes are relatively small and do not affect the main conclusions from the comparison with observations.

The combination of an underestimate in the amount of ice and an overestimate of evaporation depth-scales in the model suggests the model will significantly underestimate the evaporative cooling rate in the evaporation zone. Using the IWC at the top of the layer and the evaporation depth, an average latent heating rate for the layer can be estimated for each profile. Averaging over the whole time series of data gives a rough estimate of the average latent heating rate in the evaporation zone of -0.15 K hr^{-1} for the model compared to -1.2 K hr^{-1} ($-50\%/+100\%$) for the observations. Even if the

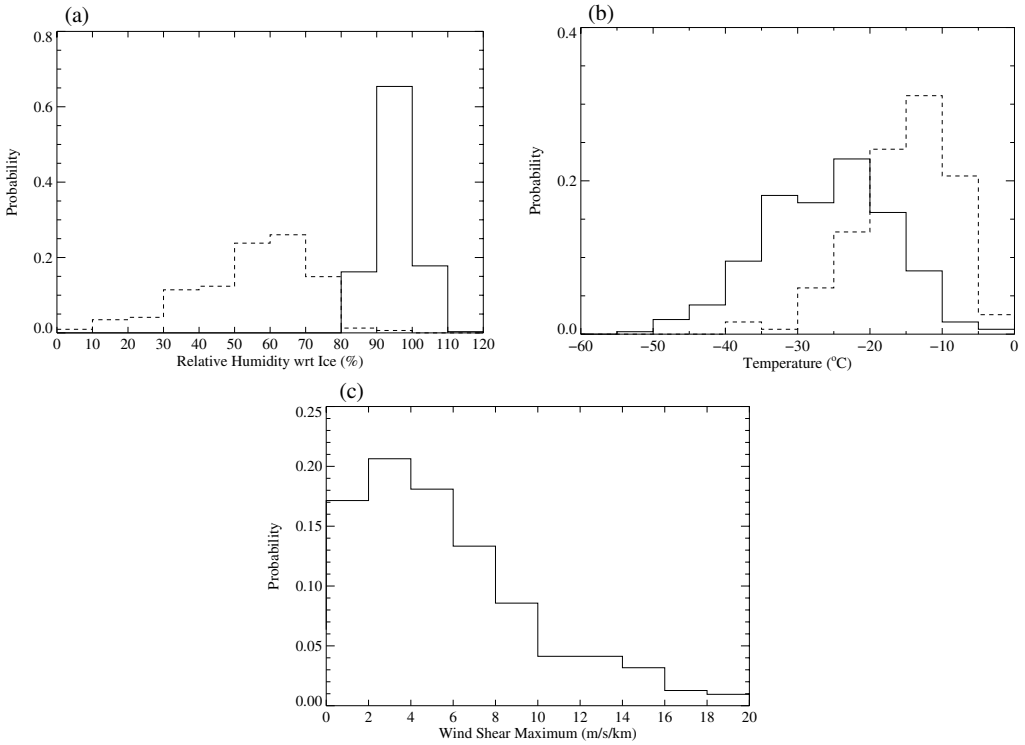

Figure 7. Probability distribution from one year of model ice evaporation profile data for (a) relative humidity (with respect to ice) at the evaporation layer top (solid) and bottom (dashed), (b) temperature at the evaporation layer top (solid) and bottom (dashed), and (c) maximum wind shear in the evaporation layer.

IWC (and therefore the latent heating rate) is underestimated by a factor of two, the model still significantly underestimates the evaporative cooling rate.

The height distributions of the top and bottom of the evaporation depths for the radar observations and the model are shown in Fig. 6(b) as cumulative probabilities. Over 95% of the observed evaporative profiles have a lower bound below an altitude of 7 km. This a posteriori justifies the choice of minimum IWC for the observation evaporative profile extraction, i.e. that the whole profile is above the minimum detectable signal for the radar which is 0.002 g m^{-3} at 7 km at the end of the time period (see section 2(b) and Fig. 1(b)). The height of the top of the evaporative zone for the model is generally higher than observed; the model average is 6.0 km compared to an observed average of 5.3 km. The model lower bound on the evaporative zone is lower than observed due to the greater evaporative depth-scales.

Information on RH, temperature and wind for each profile is also available from the model and Fig. 7 shows relevant statistics for the ice evaporation zone. The RH at the top of the evaporation zone is close to 100% with respect to ice, as expected at the base of an essentially saturated updraught (Fig. 7(a), solid line). The RH of the air that the ice is evaporating into is assumed to be the RH of the profile just below the lower bound of the evaporation zone (i.e. an additional 10% of the vertical depth-scale below the lower bound height). The RH above this level is affected by the ice evaporation itself and so this is the best available estimate of the initial humidity of the air beneath the frontal updraught. The distribution of RH at the lower bound of the evaporating profiles is shown as the dashed line in Fig. 7(a). Around 70% of the profiles have ice

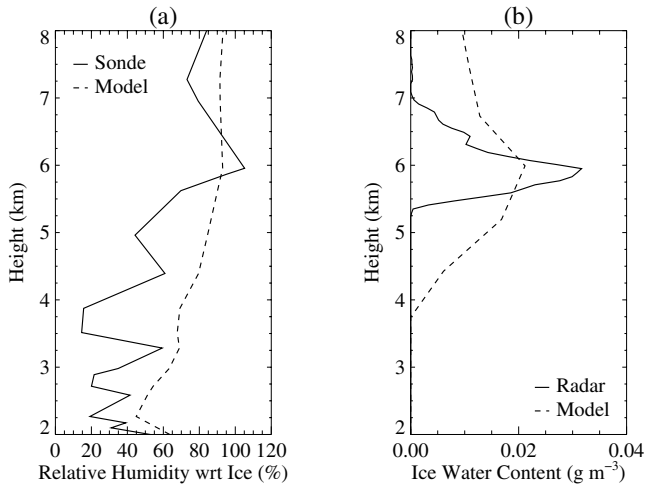

Figure 8. Vertical profiles of (a) relative humidity (with respect to ice) for the 06 UTC Larkhill radiosonde (solid) and model (dashed), and (b) ice water content derived from the 94 GHz radar and from the model for the same time on 4 August 1999.

evaporating into air with an initial RH of between 50% and 80%. The average is 60% RH. The possibility of errors in the model RH is discussed in more detail in the next section.

As expected from the distribution of heights, the range of temperatures of the upper and lower bound of the model evaporation zone is wide (Fig. 7(b)), with an average temperature of $-23\,^{\circ}\mathrm{C}$ for the upper bound and $-13\,^{\circ}\mathrm{C}$ for the lower bound. The probability distribution of the maximum wind shear in the evaporating zone in the model is shown in Fig. 7(c). Over 80% of evaporating profiles have a wind shear of less than 12 m s^{-1}km^{-1}. This suggests the horizontal averaging assumption in section 3(b), that ice particles will not be advected further than 12 km in the horizontal in the evaporation zone, is valid for the majority of cases. If the model is underestimating this shear, coarser horizontal averaging of the radar may be desirable but, as shown earlier, the impact of averaging to 4 times the horizontal distance on the evaporative depth-scales is only 10%.

(*b*) *Comparison between the model and radiosonde RH*

RH bias in the model is a possible reason why the evaporative depth-scales are overestimated compared to observations. If there is a positive RH bias in the model in the regions beneath the frontal updraughts where ice evaporation is occurring, then this will have an impact on the depth of evaporation. Of course, the process of ice evaporation itself increases the RH in this region so the two are intimately linked.

A combination of data from the 94 GHz radar at Chilbolton and the RH profile data from radiosonde ascents at Larkhill (25 km from Chilbolton) is used to determine which sondes ascended through a frontal ice evaporation zone. Data from 45 Väisälä RS80 radiosondes were extracted from the May 1999 to April 2000 period and compared with RH profiles from the model valid at the same times as the radiosondes. An example of the vertical profiles of RH (with respect to ice) for the radiosonde and model through an evaporation zone is shown in Fig. 8(a). The profiles of IWC from the radar and model for the same time are shown in Fig. 8(b). The much deeper evaporation depths in the model compared to observations is evident in this particular example.

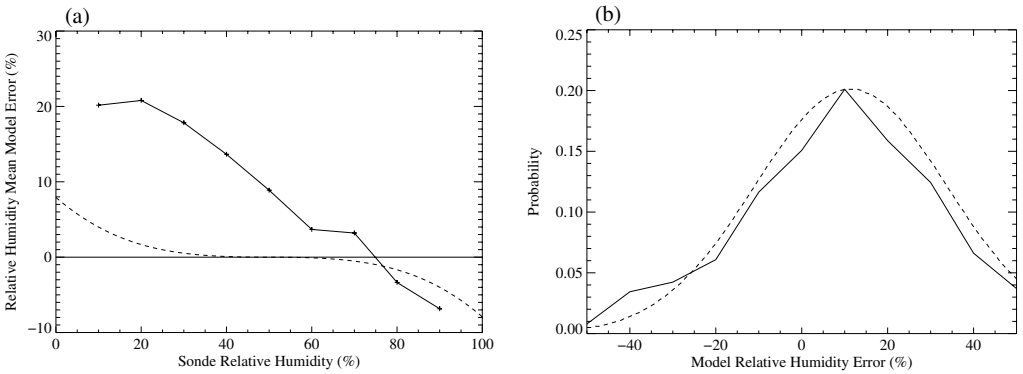

Figure 9. Statistics of the difference between the model and Larkhill radiosonde relative humidity data for 45 sondes through an evaporating zone during the one-year period from May 1999 to April 2000: (a) uncorrected model bias (solid) and bias due to the limiting values at 0% and 100% (dashed), as a function of RH from the sonde, and (b) the probability distribution of the model minus sonde RH (solid) for sonde RH values between 40% and 60%, and the Gaussian fit (dashed).

The model RH bias (with respect to ice) over all the data in the profiles is too moist by 7%, although part of this overestimate may be due to a possible dry bias of a few percent in the sonde data (Miloshevich *et al.* 2004). Given that the evaporation depth-scales are most sensitive to errors when the RH is high, the data are split into 10% RH bins. Figure 9(a) shows the model bias as a function of RH from the sonde, suggesting the model is too moist by up to 18% RH for RHs less than 75% and slightly too dry for RHs greater than 75%. However, the assumption of Gaussian statistics is invalid for very low and high RHs since there are limits at 0% and essentially 100% saturation. For example, if a particular sonde data value has a RH of just 10%, the maximum value the model-minus-sonde difference can have is −10% or +90% RH. If the model error distribution has zero bias and a standard deviation of 20%, then the negative side of the distribution will be limited to −10% RH, resulting in an apparent positive bias.

The effect of the limits on the bias can be estimated as a function of relative humidity. First a Gaussian function is fitted to the model error distribution for a RH range away from the limiting values (i.e. 40–60%). Figure 9(b) shows the model error distribution for this RH range and a Gaussian function with bias 11% RH and standard deviation 20% RH. The bias of this distribution is then assumed to be zero and the standard deviation is assumed to be valid for all other RH ranges (an analysis of half distributions close to the limiting values shows the latter to be a valid assumption). The apparent bias due to the limiting values is then calculated assuming this Gaussian error distribution is centred on RHs from 0% to 100%. The result is shown as the dotted line in Fig. 9(a). In the mid-RH range, the error distribution is not significant at the 0% and 100% RH limits, so the apparent bias is close to zero. However, as the sonde RH nears the limits, the apparent bias increases to a maximum of ±8%. The estimated 'true' bias is the model bias minus the apparent bias, i.e. the difference between the solid line and the dotted line in Fig. 9(a). Between 80% and 100% RH, the model has a small dry bias, but this is a similar magnitude to the quoted accuracy of the radiosonde data. The moist bias at RHs below 75%, which increases to a maximum of about 20% with decreasing RH, is more significant, indicating a systematic model bias in the subsaturated air beneath frontal cloud. For individual cases, the model humidity profile can be close to the observed profile, but often the drier air beneath stratiform ice cloud is too humid and the latter situation is illustrated by the example in Fig. 8.

As mentioned earlier, Miloshevich *et al.* (2004) investigated the humidity bias in Väisälä RS80 sondes and found a dry bias of a few percent due to calibration, sensor polymer contamination and time-lag errors, but even taking these into account, the model still shows a significant moist bias at RHs below 60%. The time-lag error can lead to a dry bias in this case because the radiosonde is ascending through the evaporation zone from dry to moist regions. The comparison of sonde data with the model humidity for evaporation zones was repeated with aircraft dropsondes (containing the same RS80 humidity sensor) from the 1997 FASTEX campaign (Clough *et al.* 2000), and in this case a moist bias in the sonde data may be expected because the sondes are descending through the evaporation zone. Although the data sample was smaller and the results are for a different time and location, the comparison (not shown here) has a very similar signal to Fig. 9(a), again suggesting the model has a moist bias for RH below 70% which increases with decreasing RH.

5. Discussion

The method of profile extraction is designed to isolate those parts of passing stratiform frontal cloud with ice particles falling into subsaturated air below the frontal surface. Heymsfield and Donner (1990) used a model of the ice evaporation zone to calculate the survival distance of the largest observed ice crystal particles for a given IWC over a range of temperatures and humidity subsaturations. Over the range of temperatures (0 °C to −40 °C) and IWCs (<0.2 g m^{-3}) applicable to this study, the maximum survival distance was found to be less than 1 km for a range of relative humidities. Clough and Franks (1991) showed with a simple model of ice evaporation that snow evaporates 95% of its mass in a distance of less than 500 m when the RH with respect to ice is 60% for temperatures close to 0 °C. Although a direct comparison of these results with the results from this study is not possible without additional information on the RH coincident with the continuous time series of radar data, the observation depth-scale statistics are consistent with the modelling study of Heymsfield and Donner (1990) and Clough and Franks (1991), and confirm the general hypothesis that the majority of ice particles falling from beneath a frontal surface evaporate within a depth of less than 1 km.

If we assume that the cloud is in a steady state for a few hours, then we expect a change in the static stability of a few K $m^{-1}hr^{-1}$, which under many circumstances will be large enough to destabilize the atmosphere to enhance slantwise convection or initiate vertical convection. The comparison between the model and radar evaporation depth-scales shows that the model overestimates the depth-scales by a factor of between two and three. Combined with the low IWCs, this results in a significant underestimate of the cooling rate in the evaporation layer in the model, with an associated underestimate in the dynamical response.

There are a number of possible reasons for the model error including:

- the model vertical grid resolution is inadequate. The operational model has a vertical grid spacing of between 500 and 750 m between 3 and 8 km altitude, and so it is not possible for the model to resolve depth-scales less than this.
- the RH in the model is too high beneath the frontal surface. This leads to an evaporation rate that is too low and greater evaporation depth-scales.
- the parametrized ice particle terminal fall speed is too high or the numerics are too diffusive. The fall speed of ice will affect the amount of ice and the depth the ice falls before evaporating. Numerical inaccuracies in the ice sedimentation may lead to artificially increased fall speeds.

• the parametrized ice particle evaporation rate is too low, leading to ice falling further before it evaporates.

The first hypothesis is perhaps the most obvious, i.e. limiting the minimum depth-scale to the model vertical layer depths, although the parametrization is capable of evaporating all ice within one layer if the atmospheric conditions are appropriate. The second hypothesis has been partly addressed in this paper. The comparison with the radiosonde data in evaporating zones suggests there is a significant moist RH bias in the model, although such errors may be tied up with the evaporation process itself. The impact that errors in parametrized particle characteristics, such as fall speed and evaporation rate, can have on the frontal evaporation zone and their dynamical consequences were investigated by Forbes and Clark (2003), but they did not explicitly relate the changes to changes in the evaporative depth-scales. Further investigation of the effects of model resolution, RH bias and errors in the parametrization of microphysics on the evaporation depth-scale is left to a subsequent paper.

6. Conclusion

This paper describes a statistical analysis of evaporative depth-scales beneath stratiform ice cloud from a year-long time series of radar and NWP model data from 1999 to 2000. Vertical profiles considered to contain a layer of evaporating ice are extracted from a time series of data from a vertically pointing 94 GHz radar and the Met Office operational mesoscale model at Chilbolton in the south of UK. The ice evaporative depth-scale, IWC and RH statistics from the model are compared with equivalent statistics from the radar observations and nearby radiosondes. The results lead to the following conclusions:

• Regions of significant ice evaporation from stratiform cloud are present approximately 5% of the time in both the radar and model data.

• In the radar data, 90% of the mass of ice evaporates within a depth of less than 1 km for the vast majority of profiles. This result is consistent with results from stand-alone ice cloud evaporation models (Harris 1977; Heymsfield and Donner 1990; Clough and Franks 1991).

• The model overestimates the ice evaporation depth-scales by a factor of between 2 and 3.

• The model significantly underestimates the IWC at the top of the evaporation zone. The estimate of IWC derived from radar reflectivity suggests the model underestimates the IWC by a factor of 2 to 4 in the evaporative layer, although there is still uncertainty of around $-50\%/+100\%$ in the IWC in the evaporating zone calculated from the radar.

• The combined effect of low IWC and high evaporative depth-scales in the model leads to an average cooling rate significantly less than that suggested by the observations (by at least a factor of 4). Even taking into account the factor of two uncertainty in the observation-derived IWC, the model cooling rate is still too small and will have an impact on the diabatically enhanced downdraughts in the evaporation zone (Forbes and Clark 2003).

• There is a moist RH bias in the model beneath evaporating frontal ice cloud which increases with subsaturation from a few percent at 70% RH to around 20% at lower RHs. Given that the initial RH in the evaporation layers is estimated to be less than 70% for over half the time, this may have a significant impact on the evaporation depth-scales.

The aim of this paper is to document statistics of the evaporation zone beneath frontal ice cloud from a 94 GHz cloud radar and assess the ability of a NWP model to represent the evaporation zone. Significant discrepancies between the model and observations suggest areas for model improvements which may lead to improvements in forecasting the dynamics of frontal cyclones (Clough *et al.* 2000; Forbes and Clough 2003; Browning 2004). Most importantly, this paper describes a methodology based on the use of long time series of observational data that could be applied to any NWP model to assess model error as the first step to improving NWP forecasts.

Acknowledgements

This work has been supported by the Met Office and the European Commission under contract ENV4-CT96-0322. We would like to thank the Radiocommunications Research Unit at the Rutherford Appleton Laboratory for providing the 94 GHz Galileo radar data. The Galileo radar was developed for the European Space Agency by Officine Galileo, the Rutherford Appleton Laboratory and the University of Reading, under ESTEC Contract No. 10568/NL/NB. We are also grateful to Anthony Illingworth (Meteorology Department at the University of Reading) and Peter Clark (Joint Centre for Mesoscale Meteorology) for helpful discussions, and the referees for their constructive criticisms and comments.

References

Atlas, D., Matrosov, S. Y., Heymsfield, A. J., Chou, M. D. and Wolff, D. B. 1995 Radar and radiation properties of ice clouds. *J. Atmos. Sci.*, **34,** 2329–2345

Brown, P. R. A. and Francis, P. N. 1995 Improved measurements of the ice water content in cirrus using a total-water probe. *J. Atmos. Oceanic Technol.*, **12,** 410–414

Brown, P. R. A., Illingworth, A. J., Heymsfield, A. J., McFarquhar, G. M., Browning, K. A. and Gosset, M. 1995 The role of spaceborne millimetre-wave radar in the global monitoring of ice cloud. *J. Atmos. Sci.*, **34,** 2346–2366

Browning, K. A. 2004 The sting at the end of the tail: Damaging winds associated with extratropical cyclones. *Q. J. R. Meteorol. Soc.*, **130,** 375–400

Clough, S. A. and Franks, R. A. A. 1991 The evaporation of frontal and other stratiform precipitation. *Q. J. R. Meteorol. Soc.*, **117,** 1057–1080

Clough, S. A., Lean, H. W., Roberts, N. M. and Forbes, R. M. 2000 Dynamical effects of ice sublimation in a frontal wave. *Q. J. R. Meteorol. Soc.*, **126,** 2405–2434

Cullen, M. J. P. 1993 The unified forecast/climate model. *Meteorol. Mag.*, **122,** 81–94

Forbes, R. M. and Clark, P. A. 2003 Sensitivity of extratropical cyclone mesoscale structure to the parametrization of ice microphysical processes. *Q. J. R. Meteorol. Soc.*, **129,** 1123–1148

Fox, N. I. and Illingworth, A. J. 1997 The potential of a spaceborne cloud radar for the detection of stratocumulus clouds. *J. Atmos. Sci.*, **36,** 676–687

Harris, I. 1977 The effects of evaporation at the base of ice precipitation layers: Theory and radar observations. *J. Atmos. Sci.*, **34,** 651–672

Heymsfield, A. J. and Donner, L. J. 1990 A scheme for parameterizing ice-cloud water content in general circulation models. *J. Atmos. Sci.*, **47,** 1865–1877

Heymsfield, A. J. and Miloshevich, L. M. 2003 Parameterizations for the cross-sectional area and extinction of cirrus and stratiform ice cloud particles. *J. Atmos. Sci.*, **60,** 936–956

Heymsfield, A. J. and Platt, C. M. R. 1984 A parameterization of the particle size spectrum of ice cloud in terms of ambient temperature and the ice water content. *J. Atmos. Sci.*, **41,** 846–855

Hogan, R. J., Illingworth, A. J. and Sauvageot, H. 2000 Measuring crystal size in cirrus using 35- and 94-GHz radars. *J. Atmos. Oceanic Technol.*, **17,** 27–37

Hogan, R. J., Bouniol, D., Ladd, D. N., O'Connor, E. J. and Illingworth, A. J. 2003 Absolute calibration of 94/95-GHz radars using rain. *J. Atmos. Oceanic Technol.*, **20,** 572–580

Hogan, R. J., Mittermaier, M. P. and Illingworth, A. J. 2006 The retrieval of ice water content from radar reflectivity factor and temperature and its use in evaluating a mesoscale model. *J. Appl. Meteorol. Climatol.*, **45,** 301–317

Intrieri, J. M., Stephens, G. L., Eberhard, W. L. and Uttal, T. 1993 A method for determining cirrus cloud particle size using lidar and radar backscatter technique. *J. Atmos. Sci.*, **32,** 1074–1082

Johnson, D. E., Wang, P. K. and Straka, J. M. 1993 Numerical simulation of the 2 August 1981 CCOPE supercell storm with and without ice microphysics. *J. Appl. Meteorol.*, **32,** 745–759

Liebe, H. J. 1985 An updated model for millimeter wave propagation in moist air. *Radio Sci.*, **20,** 1069–1089

Liebe, H. J., Manabe, T. and Hufford, G. A. 1989 Millimeter-wave attenuation and delay rates due to fog/cloud conditions. *IEEE Trans. Antenn. Propag.*, **37,** 1617–1623

Liu, C.-L. and Illingworth, A. J. 2000 Toward more accurate retrievals of ice water content from radar measurements of clouds. *J. Appl. Meteorol.*, **39,** 1130–1146

Miloshevich, L. M., Paukkunen, A., Vömel, H. and Oltmans, S. J. 2004 Development and validation of a time-lag correction for Väisälä radiosonde humidity measurements. *J. Atmos. Oceanic Technol.*, **21,** 1305–1327

Mittermaier, M. P. and Illingworth, A. J. 2003 Comparison of model-derived and radar-observed freezing level heights: Implications for vertical reflectivity profile correction schemes. *Q. J. R. Meteorol. Soc.*, **129,** 83–96

Nelson, J. 1998 Sublimation of ice crystals. *J. Atmos. Sci.*, **55,** 910–919

Parker, D. J. and Thorpe, A. J. 1995 The role of snow sublimation in frontogenesis. *Q. J. R. Meteorol. Soc.*, **121,** 763–782

Sassen, K. 1987 Ice cloud content from radar reflectivity. *J. Clim. Appl. Meteorol.*, **26,** 1050–1053

Srivastava, R. C. 1985 A simple model of evaporatively driven downdraft: Application to microburst downdraft. *J. Atmos. Sci.*, **42,** 1004–1023

Thorpe, A. J. and Clough, S. A. 1991 Mesoscale dynamics of cold fronts: Structures described by dropsoundings in FRONTS 87. *Q. J. R. Meteorol. Soc.*, **117,** 903–941

Thorpe, A. J., Miller, M. J. and Moncrieff, M. W. 1982 Two-dimensional convection in non-constant shear: a model of midlatitude squall lines. *Q. J. R. Meteorol. Soc.*, **108,** 739–762

Wilson, D. R. and Ballard, S. P. 1999 A microphysically based precipitation scheme for the UK Meteorological Office Unified Model. *Q. J. R. Meteorol. Soc.*, **125,** 1607–1636